Published in final edited form as:
Acta Biomater. 2013 January ; 9(1): 4513–4524. doi:10.1016/j.actbio.2012.09.029.

Controlling fibrous capsule formation through long-term down-regulation of collagen type I (COL1A1) expression by nanofiber-mediated siRNA gene silencing

Pim-on Rujitanaroj[a], **Brian Jao**[b,c], **Junghoon Yang**[b,c], **Feng Wang**[d], **James M. Anderson**[b,c], **Jun Wang**[d], and **Sing Yian Chew**[a,*]

[a]School of Chemical and Biomedical Engineering, Nanyang Technological University, 637459, Singapore

[b]Department of Pathology, Case Western Reserve University, Cleveland, Ohio 44106, USA

[c]Department of Biomedical Engineering, Case Western Reserve University, Cleveland, Ohio 44106, USA

[d]Hefei National Laboratory for Physical Sciences at the Microscale and School of Life Sciences, University of Science and Technology of China, Hefei, Anhui 230027, P. R. China

Abstract

The foreign body reaction often interferes with the long-term functionality and performance of implanted biomedical devices through fibrous capsule formation. While many implant modification techniques have been adopted in attempts to control fibrous encapsulation, the outcomes remained sub-optimal. Nanofiber scaffold-mediated RNA interference may serve as an alternative approach through the localized and sustained delivery of siRNA at implant sites. In this study, we investigated the efficacy of siRNA-PCLEEP (poly(caprolactone-co-ethylethylene phosphate) nanofibers in controlling fibrous capsule formation through the down-regulation of Collagen type I (COL1A1) *in vitro* and *in vivo*. By encapsulating complexes of COL1A1 siRNA with a transfection reagent (Transit TKO) or cell penetrating peptides (CPPs), CADY or MPG, within the nanofibers (550–650 nm in diameter), a sustained release of siRNA was obtained for at least 28 days (loading efficiency ~ 60–67%). Scaffold-mediated transfection significantly enhanced cellular uptake of oligonucleotides and prolonged *in vitro* gene silencing duration by at least 2–3 times as compared to conventional bolus delivery of siRNA (14 days vs 5–7 days by bolus delivery). *In vivo* subcutaneous implantation of siRNA scaffolds revealed a significant decrease in fibrous capsule thickness at weeks 2 and 4 as compared to plain nanofibers ($p < 0.05$). Taken together, the results demonstrated the efficacy of scaffold-mediated siRNA gene-silencing in providing effective long-term control of fibrous capsule formation.

Keywords

RNA interference; Gene knockdown; Scaffold-mediated transfection; Cell penetrating peptides; Electrospinning

*Corresponding author: Division of Chemical and Biomolecular Engineering, School of Chemical and Biomedical Engineering, Nanyang Technological University, 637459, Singapore. Tel.: +65 6316 8812; Fax: +65 6794 7553. sychew@ntu.edu.sg (S.Y. Chew).

1. Introduction

The foreign body reaction (FBR) at the tissue-implant interface frequently elicits inflammation, wound healing responses and tissue fibrosis [1–3]. In general, monocytes/macrophages are activated at implant surfaces and modulate local host fibroblast function. This often leads to excessive deposition of collagen matrix around implanted devices, a phenomenon known as fibrous encapsulation [1, 2]. Consequently, the formation of fibrous capsule surrounding implants has limited their applications in the form of glial scarring around neural probes [4], fibrotic tissue formation surrounding mammary implants [5, 6], loss of glucose biosensor functionality [7], and pacemaker failure [8]. While the modification of material surface chemistry/physics [9–12] and the incorporation of biological factors and proteins [13–17] have been developed to improve the biocompatibility of implanted devices, several potential drawbacks have also been reported. The use of a hydrogel-type coating, for instance, may display poor adhesion to the substrate, unacceptable mechanical properties for some applications and pose potential safety issues due to the use of chemical cross-linking agents [9, 16]. The administration of anti-inflammatory agents, such as dexamethasone, while being able to minimize implantation-associated inflammation, can inhibit endogenous blood vessel growth [17, 18], thereby decreasing blood circulation surrounding the implant [15].

An alternative approach is to utilize RNA interference (RNAi) technology. RNAi by small-interfering RNA (siRNA) delivery has found useful applications in the treatment of cancer [19, 20] and genetic diseases [21, 22]. Its popularity stems from its ability to knockdown virtually any gene of interest, leading to the specific down regulation of the target protein. A potential target for modulating fibrous capsule formation by RNAi is collagen type I, the major component of fibrous tissues [1, 2]. We have previously demonstrated the sustained delivery of siRNA from electrospun poly(caprolactone) [23] and poly(caprolactone-co-ethylene) (PCLEEP) nanofibers [24]. The encapsulation of siRNAs protected the degradation of these labile molecules over prolonged time periods and enhanced cellular uptake by seeded cells. Nanofiber scaffolds possess similar architecture as the fibrillar components of the native extracellular matrix (ECM). The biomimicking nature of these constructs may provide physical cues to direct cell fate [25, 26]. In addition, nanofiber topography decreased *in vivo* fibrous capsule formation and enhanced host-implant integration as compared to smooth, non-porous two-dimensional surfaces [27]. We hypothesize that the sustained release of COL1A1 siRNA from these nanofibers would permit further control over *in vivo* fibrous capsule formation.

Recently, Takahashi *et al.* [28] demonstrated that delivery of siRNA against mammalian target of rapamycin (mTOR) from poly(ethylene glycol) (PEG)-based hydrogels decreased fibroblast proliferation and type I collagen mRNA expression *in vitro*. However, *in vivo*, this platform produced no significant reduction in fibrous capsule thickness and mTOR protein level. In this study, we evaluated the efficacy of COL1A1 siRNA-encapsulated PCLEEP nanofibers in reducing fibrous capsule formation through *in vitro* and *in vivo* analyses. Similar to our previous works, the transfection reagent TransIT-TKO, was used to enable efficient cellular uptake. However, in order to resolve cytotoxicity issues related to TKO [24], cell penetrating peptides (CPPs) were introduced as an alternative for siRNA complexation. CPPs such as MPG and CADY, are natural peptide-based molecules that mediate transfection through the formation of stable non-covalent complexes with nucleic acids, thereby improving intracellular delivery *in vitro* [29–33] and *in vivo* [29, 34, 35]. In addition, CPPs induced less cytotoxicity as compared to cationic lipid-based molecules [36–38] and cationic polymers [38–40]. We evaluated the functionality of PCLEEP nanofibers that encapsulated COL1A1 siRNA-CPP complexes. Such siRNA nanofibers may find useful

applications as direct implantable scaffolds or surface modifications to improve tissue-implant integration of medical devices.

2. Materials and methods

Poly (ε-caprolactone-co-ethyl ethylene phosphate) (PCLEEP, M_w: 94,000 and M_n: 48,000) with 1% ethyl ethylene phosphate (EEP) was synthesized through bulk ring-opening polymerization of ε-caprolactone and EEP as reported previously [41, 42]. Scrambled negative siRNA (denoted as siNEGCy5-labeled oligonucleotides (Cy5-ODN) DEPC-treated PBS (pH 7.4), DEPC-treated Tris-EDTA (TE) buffer (pH 8.0), DEPC-treated water and CPPs (purity > 90%) were purchased from 1st Base, Singapore. The CPPs, MPGΔ^{NLS} (GALFLGFLGAAGSTMGAWSQPKSKRKV) and CADY (GLWRALWRLLRSLWRLLWRA), were acetylated at their N-terminus and synthesized with a cysteamide group at their C-terminus. Silencer® COL1A1 siRNA (denoted as siCOL1A1) targeting the human (NM_000088.3) and rat (NM_053304) COL1A1 genes was purchased from Ambion (ID #: s3276), USA. Transfection reagent, TransIT-TKO, was obtained from Mirusbio, USA. RiboGreen® reagent Quanti-IT™ RiboGreen, TRIzol® reagent, 40,6-Diamidino-2-phenylindole (DAPI), Oregon Green® Phalloidin 488 and Alexa Fluor® 488 donkey anti-goat IgG were purchased from Invitrogen, USA. Ethidium bromide solution and iQ SYBR Green Supermix were purchased from Bio-Rad Laboratories, USA. Goat anti-human collagen type I was purchased from Millipore, USA. Human dermal fibroblasts (HDFs) were purchased from Lonza, Basel, Switzerland. Dulbecco's Modified Eagle's Medium (DMEM) and fetal bovine serum (FBS) were obtained from Hyclone, USA. Penicillin-streptomycin (10 000 U/mL), antibiotic-antimycotic and phosphate buffered saline (PBS, pH 7.4) were purchased from Gibco, Invitrogen, USA. RQ1 RNase–free DNase, and Sensiscript® RT kit were purchased from Promega, USA, and Qiagen Germany, respectively. Poly (ε-capolactone) (PCL, M_w: 65,000), bovine serum albumin (BSA), 2,2,2-trifluoroethanol (TFE, ≥99.0), tetrahydrofuran (THF, ≥99.9), chloroform (≥99.9), dimethyl sulfoxide (DMSO), Triton X-100, 10% formalin and 100% ethanol were obtained from Sigma-Aldrich, USA. Aerrane® isoflurane was obtained from Baxter Healthcare Corporation, Deerfield, Illinois, USA. Betadine was obtained from The Purdue Frederick Co., Stamford, CT, USA. 0.5% Marcaine solution was obtained from Abbott Laboratories, North Chicago, IL, USA. All chemicals were used as received without any further purification.

2.1 Electrospinning of siRNA-encapsulated PCLEEP nanofibers

Plain PCLEEP nanofibers (control group denoted as PCLEEP) and PCLEEP nanofibers encapsulating siRNA/TKO complexes corresponding to a volume ratio of 1/2 (denoted as siNEG/TKO and siCOL1A1/TKO when scrambled negative siRNA and siRNA targeting COL1A1 were added, respectively) were fabricated according to our previous work [24].

To obtain PCLEEP nanofibers that encapsulated siRNA/CPP complexes, a 20% w/v PCLEEP-TFE solution was prepared. siNEG or siCOL1A1 was reconstituted in RNase free water to obtain a stock solution of 50 μM concentration. Thereafter, 15 μL of siRNA was mixed with either 30 μL, 45 μL or 60 μL of CPP (350 μM of MPG in DEPC-treated water and 370 μM of CADY in 2% DMSO-DEPC-treated water) to obtain volume ratios of 1/2, 1/3 or 1/4 respectively. Thereafter, the mixture was incubated for 20 min and DEPC-treated TE buffer was then added to obtain a final volume of 100 μL. The siRNA/CPP mixture was then added into 500 μL of PCLEEP solution. The uniform siRNA/CPP-polymer mixture was dispensed using a syringe pump (New Era Pump) at a flow rate of 1.5 ml/h through a 21G needle and charged at +12 kV (GAMMA high voltage research, USA) for electrospinning. The polymer supply was set at 12 cm away from the target. A negatively charged stationary aluminum foil (−4 kV, 5 × 5 cm^2) was used as the target for randomly-oriented nanofibers.

In order to obtain aligned PCLEEP nanofibers for *in vivo* studies, the fibers were deposited directly onto a PCL film that was mounted on a grounded rotating target (2500 rpm). The spinning process was carried out at 20–23°C and the humidity was 54–58%. The PCL film was obtained by solvent casting 0.15 g/ml of PCL-chloroform solution overnight, followed by lyophilization for 12 hours to remove any residual solvents. PCLEEP nanofibers that encapsulated complexes of siNEG with MPG or CADY; and siCOL1A1 with MPG or CADY were fabricated and denoted as siNEG/MPG, siNEG/CADY, siCOL1A1/MPG and siCOL1A1/CADY, respectively. Table 1 summarizes all electrospun nanofiber samples that were prepared for this study, along with their notations and processing parameters.

2.2 Evaluation of scaffold morphology and ODN distribution

PCLEEP, siCOL1A1/MPG, siCOL1A1/CADY and siCOL1A1/TKO nanofiber scaffolds were sputter coated with platinum and evaluated by scanning electron microscopy (SEM) (JOEL, JSM-6390LA, Japan) at 5000× magnification. The average fiber diameters were then determined using Image J (NIH, USA) by measuring 100 fibers per sample. In order to evaluate the distribution of siRNA inside PCLEEP nanofibers, Cy5-ODN was used. Briefly, Cy5-ODN-encapsulated (1/4 volume ratio) nanofibers were incubated with 500 μL of complete cell culture medium for 24 h. Thereafter, the scaffolds were washed three times with PBS, mounted onto glass slides using fluoromount and imaged by confocal microscopy (Zeiss, LSM 710 Meta Laser Scanning Confocal Microscope, Germany).

2.3 Cell culture

HDFs were cultured in complete medium comprising of DMEM supplemented with 10% FBS and 1% penicillin-streptomycin. Cells were maintained in a humidified incubator at 37 °C with 5% CO_2. The HDFs were kept within passage 15 to 30 to ensure similar cellular activity for siRNA transfection.

2.4 Optimization of siRNA/CPP complexation ratio

In order to identify the combination of CPPs and siRNA for optimal complexation and cellular uptake, agarose gel-shift assay and visualization of Cy5-ODN uptake by HDFs were conducted. Firstly, stock solutions of MPG (350 μM in DEPC-treated water) and CADY (370 μM in 2% DMSO-DEPC-treated water) were prepared and the siRNA concentration was set at 50 μM. Thereafter, siRNA/CPP molar ratio variation was adopted for typical bolus delivery on glass cover slips (two-dimensional (2D) controls) for ease of comparison with the literature. For scaffold-mediated transfection, volume ratio variation was used for ease of sample preparation during the electrospinning process.

2.4.1 Agarose gel-shift assay—SiNEG/MPG and siNEG/CADY complexes were incubated for 30 min at room temperature in DEPC-treated TE buffer at molar ratios between 1/10 and 1/80 or volume ratios between 1/3 and 1/10. Thereafter, 20 μL of the stable complexes was loaded for agarose gel electrophoresis (1 %wt/vol stained with ethidium bromide), and UV-visualization (ChemiDoc™ XRS, Bio-Rad Laboratories).

2.4.2 Cy5-ODN uptake by HDFs—Two modes of transfection were used in this study - bolus delivery on 2D surface (control) and scaffold-mediated transfection. In the former, HDFs were cultured on glass cover slips and transfected with Cy5-ODN/CPP complexes at a molar ratio of 1/40, 1/60 or 1/80. In the latter, cells were cultured on Cy5-ODN/CPP-encapsulated nanofiber scaffolds that comprised of Cy5-ODN/MPG or Cy5-ODN/CADY complexes at a volume ratio 1/2, 1/3 or 1/4. Due to possible photobleaching of Cy5, the scaffolds were not sterilized under UV. Instead, 1% antibiotic-antimycotic solution was added into the culture medium to prevent contamination. In both setups, HDFs were seeded

at a density 3.5×10^4 cells/cm^2 in 24-well plates with 500 μL of complete medium for 4 hours prior to transfection. Twenty-four hours after transfection, all samples were fixed with 10% formalin for 30 min at room temperature, permeabilized in 0.3% Triton X-100 for 20 min and stained with DAPI (1:1000) and Oregon Green® Phalloidin 488 (1:500) for 30 min. The uptake of Cy5-ODN was then observed by confocal microscopy. In order to quantify Cy5-ODN intensity, each individual cell was outlined and Cy5-ODN signal intensity was measured using Image J by measuring 20 cells per sample. The measurement was repeated for 3 samples per group, resulting in a total of 60 cells per group.

2.5 Analysis of siRNA release kinetics

The release kinetics studies and the experimental loading efficiency of siRNA were evaluated based on a previous protocol [24]. Scaffolds encapsulating siNEG/MPG (1/4 volume ratio), siNEG/CADY (1/4 volume ratio) and siNEG/TKO (1/2 volume ratio) (average weight = 75 ± 5 mg, n=3) were used in this study and were incubated at 37 °C with shaking speed of 70–90 rpm.

2.6 Evaluation of long-term siRNA gene silencing efficiency by bolus delivery and scaffold-mediated delivery

2.6.1 Bolus delivery of siRNA—One day before transfection, HDFs were plated onto glass cover slips at a density of 5×10^3 cells/cm^2 in 12-well plates with 500 μL of complete medium. Twenty-four hours later, cells were approximately 40–50% confluent. CPP (MPG or CADY) and TKO were used for the transfection of HDFs according to Simeoni *et al.* [43] and the manufacturer's protocol respectively with slight modifications. For transfection using CPP, a concentration of 20 nM siRNA was complexed with CPP corresponding to a molar ratio of 1/60 for 20 min at room temperature to allow complex formation. DMEM was then added to obtain a total volume of 400 μL and incubated for 10 min. For transfection using TKO, 3 μL of TKO reagent was complexed with 20 nM of siRNA for 20 min at room temperature and DMEM was then added to obtain a final volume of 400 μL. Thereafter, cells were overlaid with 400 μL of siRNA/CPP or siRNA/TKO complexes and incubated at 37 °C for 30 min. 600 μL of complete media was then added into each well to achieve the final transfection volume of 1 mL/well. Forty-eight hours after transfection, the medium was replaced with fresh complete medium and incubated until day 3, day 5 and day 7 with half of the medium changed every 3 days. The negative controls comprised of cells that were treated with siNEG/CPP or siNEG/TKO complexes. Eight wells of cells were pooled for each sample and COL1A1 mRNA expression levels were evaluated by real-time PCR or immunostaining. The entire transfection experiment was repeated 3 times. For glass (control) sample by immunostaining analysis, cells were plated at the same density without transfection and cultured until day 3, day 5 and day 7 with half of the medium changed every 3 days.

2.6.2 Scaffold-mediated transfection—PCLEEP nanofibers that encapsulated siRNA/MPG (1/4 volume ratio), siRNA/CADY (1/4 volume ratio) and siRNA/TKO (1/2 volume ratio) were used for scaffold-mediated transfection. The scaffolds (n=8, average weight of 70 mg) were cut to fit the wells of 12-well plates and sterilized under UV for 1 h. HDFs were seeded on the scaffolds at 5×10^3 cells/cm^2 in 1 mL of complete medium. Cells were cultured on the scaffolds for 3, 7 and 14 days with half of the medium changed every 3 days. As the negative controls, cells were cultured on siNEG/MPG (1/4 volume ratio), siNEG/CADY (1/4 volume ratio) or siNEG/TKO (1/2 volume ratio) scaffolds. At specific time points, cells were harvested for real-time PCR or immunostaining. The entire transfection experiment was repeated 3 times. To prepare PCLEEP (control) samples for immunostaining, cells were seeded onto plain PCLEEP scaffolds at the same density and cultured for 3, 7 and 14 days with half of the medium changed every 3 days.

2.7 RNA analysis and real-time RT-PCR

Cells were lysed using TRIzol® reagent and RQ1 RNase–free DNase was added to the isolated RNA to improve RNA quality. Reverse transcription was carried out using Sensiscript® RT kit according to manufacturer's protocol. COL1A1 mRNA expression levels were determined by real-time PCR using StepOnePlus™ Real-time PCR systems (Applied Biosystems), with β-actin as the housekeeping gene. The primer sequences for COL1A1 gene were: forward 5′-CAATGCTGCCCTTTCTGCTCCTTT-3′, reverse 5′-ATTGCCTTTGATTGCTGGGCAGAC-3′ and the product size was 125 bp. The primer sequences for β-actin were: forward 5′-GGCACCCAGCACAATGAAGATCAA-3′, reverse 5′-ACTCGTCATACTCCTGCTTGCTGA-3′, and the product size was 134 bp. The real-time PCR condition used was as follows: 3 min at 95 °C, 40 cycles at 95 °C for 15 s, followed by 60 °C for 30 s. Our preliminary studies showed that these two primers had similar amplification efficiencies under the parameters used and therefore the ΔΔCT method was chosen to compare mRNA levels. All results were normalized with respect to the mRNA expression of the corresponding negative controls at each time point. The entire COL1A1 gene silencing experiment was repeated 3 times for each sample.

2.8 Immunocytochemistry

Transfected cells were stained at specific time points by COL1A1 antibody. Briefly, samples were washed once in PBS and fixed with 10% formalin solution for 1 h at room temperature. Non-specific sites were blocked three times in PBS with 1% BSA (blocking solution) for 30 min. Cells were incubated overnight with goat anti-collagen type I antibody (1:50) in blocking solution. After washing three times with PBS, immunostaining was revealed by incubation for 2 h with Alexa Fluor® 488 donkey anti-goat antibody (1:200) in PBS. Nuclei were counterstained with DAPI (1:1000) and the samples were then mounted on glass slides using fluoromount and imaged by confocal microscopy.

2.9 *In vivo* studies

2.9.1. Surgical implantation—Based on our previous work [27], aligned electrospun nanofibers minimized host response, enhanced tissue-scaffold integration as compared to randomly oriented nanofibers and elicited a thinner fibrous capsule than 2D film substrates. Therefore, aligned PCLEEP nanofibers were used for scaffold-mediated COL1A1 silencing *in vivo*. Due to the poor mechanical property along the direction perpendicular to fiber alignment, all nanofibers were supported on a film to ease implantation. The average thickness of PCL film was 70.2 ± 8 μm as evaluated by SEM. All materials were sterilized under UV for 1 h prior to implantation. In addition, since no non-specific knockdown of COL1A1 was observed in HDFs when treated with scrambled siRNA and transfection reagents during our *in vitro* studies (Supplementary Fig. 1). The scrambled controls were not included in the *in vivo* experiments.

All procedures were approved by the Institutional Animal Care and Use Committee (IACUC) and NIH Animal Care Guidelines of Case Western Reserve University. Samples of each material (1 × 2 cm^2) were implanted subcutaneously, two per animal, in the posterior back areas of female Sprague-Dawley rats (6 to 8 weeks old, Charles Rivers Laboratories, North Wilmington, MA, USA) for 2 and 4 weeks. A total of 3 animals were used for each group at each time point. The animal studies were conducted according to our previous protocol [44]. Briefly, the rats were anesthetized by gaseous mixture of Aerrane® isoflurane during implantation. Their backs were shaved and cleaned with surgical grade Betadine followed by 100% ethanol. An incision 1.2 cm length was made in the skin about 2 cm above the tail and along the midline. Subcutaneous pockets on both sides of incisions were created by blunt curved forceps and the sterilized material was then introduced through the incision and positioned within the pocket and away from the incision site. The insertion

procedure was repeated for the opposite side. The incision was then closed with 9 mm stainless steel surgical wound clips (Becton Dickinson, Spark, MD, USA) and a small amount of 0.5% Marcaine solution was applied onto the incision to minimize post-operative discomfort. The rats were maintained on Purina Rat Chow and water at the Animal Research Facilities of Case Western Reserve University on 12 h light/dark cycles.

2.9.2. Histological Evaluation—Histological analysis was performed on the explanted tissues at 2 and 4 weeks using a previous protocol [45]. In particular, fibrous capsule measurements were taken in the middle part of the section to reduce artifacts such as the motion effect and end effects. Fibrous capsule thickness and cell infiltration for each section was measured as the average thickness at ten different random locations and was determined as the average thickness of three sections per explant. Three explants were measured for each group. Therefore, ninety measurements were determined in each group at each time point. The stained sections were visualized using light microscopy (Olympus, model No.: IX71) under 4× or 10× magnifications. The thickness of fibrous capsule and cellular infiltration were measured using H & E stained images and confirmed with Masson's Trichrome stained images. ImageJ was used for all measurements.

2.10. Statistics

All quantitative values were expressed as a mean ± standard error (SE) of the mean. Statistical comparisons for fiber diameter, siRNA release kinetics and silencing efficiency were performed using one-way ANOVA and Tukey post-hoc tests after verifying equal variances otherwise non-parametric test was used for unequal variances. The student's t-test was used for statistical comparisons involving 2 samples. $P < 0.05$ was considered statistically significant.

3 Results

3.1 Optimization of siRNA/CPP complexes

In order to evaluate the stability of the siRNA/CPP complexes, agarose gel-shift assay was conducted. As indicated in Fig. 1a, siRNA bands were detected when the molar ratios were less than or equal to 1/10 and 1/20 for CADY and MPG respectively, indicating the presence of uncomplexed siRNA. As shown in Fig. 1b, free siRNA was not detected at volume ratios ≥ 1/3. These results suggested that above these molar and volume ratios, all siRNA molecules are completely entrapped in CPP complexes through electrostatic interactions. Therefore, molar ratio ≥ 1/40 and volume ratio ≥ 1/3 were used in subsequent experiments.

3.2 Morphology of siRNA/CPP- and siRNA/TKO-encapsulated nanofibers

As shown in Fig. 2a–b and Supplementary Fig. 2, randomly-oriented and aligned PCLEEP nanofibers with uniform diameters were obtained. The average diameters of randomly-oriented PCLEEP, siCOL1A1/MPG, siCOL1A1/CADY and siCOL1A1/TKO nanofibers were 652 ± 16 nm, 649 ± 8 nm, 636 ± 11 nm and 631 ± 14 nm, respectively, with no significant difference. Comparatively, significantly smaller fiber diameters were observed for aligned nanofibers (554 ± 14 nm, 560 ± 23 nm, 570 ± 20 nm and 563 ± 15 nm for PCLEEP, siCOL1A1/MPG, siCOL1A1/CADY and siCOL1A1/TKO nanofibers, respectively, $p < 0.05$), likely due to the mechanical stretching that was imparted during the fiber alignment process. As shown in Fig. 2c, Cy5-ODN signals were detected along the polymer fibers even after 24 h incubation in culture medium and multiple washes in PBS. This indicated that the ODN/CPP complexes were successfully encapsulated within the nanofibers.

3.3 Cellular uptake of Cy5-ODN uptake by bolus delivery and scaffold-mediated transfection

In order to determine the ideal amount of CPP for optimal cellular uptake of oligonucleotides (ODN), Cy5-ODN was used as the model oligonucleotide for visualization. Fig. 3a – f and 3g – l illustrate the extent of cellular uptake of Cy5-ODN by bolus delivery and scaffold-mediated transfection, respectively. As demonstrated in Fig. 3(a–f), bolus delivery resulted in Cy5-ODN aggregates within HDFs. In addition, Cy5-ODN uptake varied with siRNA/CPP molar ratio. Within the range analyzed, 1/60 appeared to be the optimal molar ratio for transfection via bolus delivery of CADY and MPG (Fig. 3m), and was thus used for all subsequent experiments. At all molar ratios, CADY consistently enhanced cellular uptake as compared to MPG ($p < 0.05$).

As compared to bolus delivery, scaffold-mediated transfection significantly enhanced cellular uptake (Fig 3m, $p < 0.05$). Cy5-ODN signals appeared diffused in HDFs that underwent scaffold-mediated transfection (Fig. 3g–l). No significant difference was observed between CADY and MPG. Since a general increase in Cy5-ODN uptake was observed as siRNA/CPP volume ratio increased, the volume of 1/4 was used for all subsequent analyses.

3.4 Release kinetics of siRNA

Sustained release of siRNA was detected for up to 28 days after initial burst release upon immersion into PBS at time, t = 0 (Fig. 4). No significant difference was detected among samples at t = 0. However, at t = 24 h, the release of siRNA from siNEG/MPG, siNEG/CADY and siNEG/TKO nanofibers were significantly different (66.8 ± 2%, 76.6 ± 1% and 46.8 ± 1%, $p < 0.05$ respectively). In terms of concentrations, these values were equivalent to 5.02 nM, 5.75 nM and 3.76 nM, respectively. At day 49, the total amount of siRNA that was released from siNEG/MPG and siNEG/CADY were 90.1 ± 3% and 92.1 ± 2% respectively. Comparatively, siNEG/TKO nanofibers released the lowest amount of siRNA throughout the period of study (80.6 ± 2% at 49 days). The experimental loading efficiencies for siRNA/MPG, siRNA/CADY and siRNA/TKO samples were 65.8 ± 3%, 67.2 ± 4% and 60.4 ± 2%, respectively, suggesting that CPP and TKO complexation did not significantly alter the loading efficiency of siRNA.

3.5 Long-term gene silencing efficiency by bolus delivery and scaffold-mediated transfection

Bolus delivery of siCOL1A1 complexes significantly decreased COL1A1 expression (Fig. 5a). At day 3, gene knockdown efficiencies of ~ 19.4%, 39.0% and 81.3% were detected for siCOL1A1/MPG, siCOL1A1/CADY and siCOL1A1/TKO samples, respectively, and the results were significant as compared to the respective negative controls. By day 5, COL1A1 expression level returned to normal for the siCOL1A1/MPG sample while siCOL1A1/CADY and siCOL1A1/TKO samples displayed normal levels of COL1A1 by day 7. At each time point, the silencing efficiencies demonstrated a similar trend: TKO > CADY > MPG, $p < 0.05$. This trend was similarly reflected at the protein level as demonstrated by immunofluorescence staining (Fig. 5b).

Fig. 5c shows COL1A1 knockdown in cells seeded directly on siCOL1A1/MPG, siCOL1A1/CADY and siCOL1A1/TKO nanofiber scaffolds. Significant down-regulation of COL1A1 gene expression was observed at day 7 as compared to the respective negative controls. No significant difference was detected between all samples. At day 14, the silencing efficiencies were significantly higher as compared to day 7 with 26.7%, 46.7% and 50.5% silencing observed for siCOL1A1/MPG, siCOL1A1/CADY and siCOL1A1/TKO samples, respectively. In general, the silencing efficiency followed the trend: TKO ~ CADY

> MPG, $p < 0.05$. This trend was similarly reflected at the protein level as demonstrated by immunofluorescence staining (Fig. 5d).

3.6 *In vivo* evaluation of fibrous capsule formation and cellular infiltration

For all scaffolds, no acute or chronic inflammation or necrosis that was indicative of toxicity was identified at any of the time periods as shown in Supplementary Fig. 3. High magnification histological evaluation (data not shown) also revealed no signs of toxicity. At each time period, the tissue response at the interface was similar for all samples and no significant difference in the resolution of the inflammatory response and development of granulation tissue and fibrous capsule was observed as expected for a biocompatible (non-toxic) material scaffold.

Fig. 6 and Supplementary Fig. 3 show the histology tissue sections. In general, the large film thicknesses reflected in the sections are mainly due to the delamination of tissues and artifacts that were introduced during the tissue sectioning process. As indicated by Masson's Trichrome staining in blue, thicker collagen deposition was found at the interface between tissues and the supporting film, as compared to nanofiber surfaces. Detailed quantitative comparisons at weeks 2 and 4 (Fig. 6e) showed that significantly thicker fibrous capsule was formed around plain PCLEEP nanofibers as compared to siCOL1A1/CADY and siCOL1A1/TKO scaffolds (Fig. 6e, $p < 0.05$). No significant difference was observed between CADY and TKO samples. Comparing the results between weeks 2 and 4, a significant decrease in fibrous capsule thickness was observed for siCOL1A1/CADY and siCOL1A1/TKO samples. In general, the overall decrease in fibrous capsule thickness profile could be ranked as: TKO ~ CADY > MPG ~ PCLEEP.

As shown in Fig. 6f and Supplementary Fig. 3, cell infiltration into aligned nanofibrous scaffolds was similar amongst samples and was approximately 20–40% after 2 weeks. This trend remained constant up to week 4. As anticipated, cell infiltration was not observed at the film interface (Fig. 6 and Supplementary Fig. 3) after 4 weeks post-implantation.

4. Discussion

Fibrous capsule formation is associated with elevated proliferation and activation of fibroblasts that up-regulate collagen production in tissues surrounding implanted materials. While many implant modification techniques have been adopted in attempt to reduce fibrous capsule formation [9–16], the outcomes remained sub-optimal [9, 16–18]. Since collagen type I is the major component of fibrous capsules, we hypothesized that the silencing of collagen type I expression would allow regulation of fibrous encapsulation. Extending from our previous work, where nanofiber topography enhanced host-implant integration and decreased fibrous capsule formation as compared to smooth nonporous film surfaces [27], we incorporated RNA interference capability into these fibers via siRNA encapsulation. The incorporation of siRNA within nanofibers protects these labile molecules from biodegradation while allowing localized and sustained availability of siRNA to seeded cells. Fabricated by the versatile electrospinning technique, these nanofiber constructs may serve as direct implantable scaffolds [46–48] or as a surface modification approach to enhance host-implant integration of medical devices [3, 27, 49]. In practical applications, siRNA-encapsulated nanofibers may be wrapped or coated onto medical devices in order to control fibrous capsule formation surrounding the implants. The modification of device surfaces by coating with nanofibers has also been reported by Ravichandran *et al.* [50] and Yang *et al.* [51]. Coating Ti surfaces with poly(lactic-co-glycolic acid) (PLGA)/collagen nanofibers resulted in the enhanced proliferation, differentiation and mineralization of human mesenchymal stem cells [50]. Deposition of conducting polymer poly(3,4-ethylenedioxythiophene) (PEDOT) onto neural electrodes also elicited favorable biological

response from SHSY5Y human neuroblastoma lines towards the material interface [51]. Since PCLEEP has demonstrated low cytotoxicity and good biocompatibility [46], the siRNA nanofibers may help in improving functionality and biocompatibility of implants.

For effective gene knockdown, siRNA must be translocated across cellular membranes upon release from nanofibers. However, common transfection agents such as Lipofectamine 2000 and TransIT TKO, while able to facilitate cellular internalization of siRNA, often induced cytotoxicity [36–38]. As reported by Andersen *et al.* [38], transfection of TransIT-TKO/siRNA complexes into H1299 human lung carcinoma cells produced a high cell mortality (only 60% of cells were viable after transfection). Similar findings were also reported in our previous work [23, 24]. In contrast, CPPs, such as MPG and CADY, promoted *in vitro* and *in vivo* cellular uptake of a variety of macromolecules including proteins, peptides and oligonucleotides with less cytotoxicity [30, 31]. Crombez *et al.*, [31] reported that siRNA/CADY complexes (molar ratios from 1/20 to 1/80) did not affect the viability of human osteosarcoma cells (U_2OS) after 24 h transfection, as demonstrated by MTT assay. Similarly, our results showed that transfection of siCOL1A1 using MPG or CADY appeared to produce significantly higher cell viability than using TKO ($p < 0.05$, Live/Dead and WST-1 assay, Supplementary Fig. 4).

As a starting step to encapsulate siRNA/CPP within electrospun nanofibers, the stability of the complexes was first evaluated. Although the agarose gel shift assay indicated the formation of stable siRNA/CPP complexes at molar ratios ≥ 1/40, optimal cellular uptake was achieved only at molar ratio 1/60 via bolus delivery. In the case of CADY, this trend also translated to gene knockdown efficiency (Supplementary Fig 5). The lack of enhancement in silencing efficiency above a 1/60 molar ratio of siRNA/CADY may be due to the aggregation and formation of large complex particles that result in poor cellular uptake [31]. In the case of MPG complexation, no significant difference in silencing effect was seen at all molar ratios (Supplementary Fig. 5). It is possible that unstable complex formation (lane 3 and 4, Fig. 1a) and degradation by nucleases [52] may have occurred.

Randomly oriented and aligned nanofibers that encapsulated siRNA complexes were successfully fabricated by electrospinning. The encapsulation of siRNA complexes into nanofibers was less than 100%, likely due to the partial loss of biomolecules during the electrospinning process. Such occurrences were also seen in other studies [23, 24]. Among scaffolds with similar fiber orientation, the average diameters of the samples were not significantly different regardless of the types of siRNA complexes present. This is likely due to the low amounts of siRNA used. The similar fiber diameters helped eliminate fiber size effect on *in vitro* and *in vivo* cellular response. Similar to our previous observations [24], the encapsulation of siRNA/CPP or siRNA/TKO within PCLEEP fibers resulted in initial burst releases of siRNA. This phenomenon is likely attributed to siRNA that was located on the surface of the nanofibers, since uniform PCLEEP-siRNA mixtures were electrospun. Comparatively, the burst releases of siRNA/CPP complexes were similar to naked siRNA encapsulation [24] and were significantly higher than siRNA/TKO complexes. Correspondingly, the rate and amount of siRNA/TKO complexes that was released were lower as compared to siRNA/CPP complexes. One possible reason may be the enhanced hydrophilicity of CPPs vs. TKO. As compared to naked siRNA [24], the experimental loading efficiencies of siRNA/CPP and siRNA/TKO complexes within PCLEEP were similar. However, the total amount of siRNA that was being released by day 49 was significantly lower in the siRNA/TKO samples.

Since fibroblasts are the major contributors to collagen secretion and *in vivo* fibrous capsule formation, *in vitro* gene silencing was first evaluated using fibroblast culture. Although the *in vitro* release of siRNA was detected after 24 hours (Fig. 4), the significant down

regulation of COL1A1 gene expression was observed at day 3 for bolus delivery and at day 7 for scaffold-mediated delivery (Fig. 5a and 5c). It is possible that the accumulation of siRNA above the threshold concentration for effective gene knockdown requires several days after delivery starts [51]. As compared to bolus delivery, scaffold-mediated transfection significantly enhanced cellular uptake despite significantly lower amounts of siRNA released as indicated by the release profiles (5 nM and 5.75 nM for MPG and CADY samples at day 1 respectively (Fig. 4) vs. 20 nM per well by bolus delivery). This is likely due to the increased local availability of ODN as cells were in direct contact with the scaffolds [23]. Bolus delivery of siRNA complexes led to transient gene silencing of 5–7 days only. Any requirement for prolonged silencing effect would necessitate multiple subsequent transfections. In contrast, scaffold–mediated transfection prolonged *in vitro* gene silencing duration by at least 2–3 times. Such prolonged and enhanced transfection efficiency by scaffolds is likely due to the sustained release and localized concentration of siRNA to cells. Similar findings were also observed previously [53, 54]. The co-encapsulation of siCOL1A1 and CADY within PCLEEP fibers resulted in similar COL1A1 knockdown as compared to siCOL1A1/TKO complexes. Combined with the more efficient sustained release of siRNA/CADY vs. siRNA/TKO, the delivery of siRNA/CADY complexes appeared more advantageous. In addition, the results also demonstrated the efficacy of siRNA encapsulated nanofibers in providing effective long-term gene silencing as compared to the conventional bolus delivery to 2D cultures.

The efficacy of scaffold-mediated gene silencing in modulating fibrous capsule formation was then verified *in vivo*. Similar to our previous finding [27] nanofibers decreased fibrous capsule formation as compared to the smooth surface of a film. It appears that scaffolds with lower porosity are more likely to induce dense fibrous capsule formation, so the thickness of the fibrous capsule can be greatly reduced when implants are more porous [10, 55, 56]. Since the fiber diameter of PCLEEP in this study was similar to PCL nanofibers [27], the porosity (~83%) would not be expected to differ significantly as well.

Attempts to modulate collagen expression in fibroblasts by gene knockdown were also made previously. Shegogue *et al.* and Takahashi *et al.* demonstrated that *in vitro* inhibition of mTOR in fibroblasts influenced cell proliferation and collagen type I production [28, 57]. However, despite the success in *in vitro* gene knockdown, the introduction of mTOR siRNA *in vivo* using PEG-based hydrogels failed to demonstrate significant reduction in protein knockdown and fibrous capsule thickness after 2 weeks [28]. In contrast, our results demonstrate a significant decrease in fibrous capsule thickness in response to CADY- and TKO-mediated delivery of siCOL1A1 at weeks 2 and 4 as compared to PCLEEP samples. Specifically, the reduction of fibrous capsule thickness at week 4 was 50.5% and 61.9% for CADY and TKO as compared to PCLEEP samples, respectively (Fig.6e). The *in vivo* knockdown efficiency of CADY and TKO as compared to MPG agreed with our *in vitro* results. Collectively, the results indicated the potential of scaffold-mediated gene-silencing for long term control of *in vivo* fibrous capsule formation. It is noted that a significant decrease in fibrous capsule thickness was observed between weeks 2 and 4 for all samples. We believe that this is likely associated with the normal wound healing process, where an increase in density of fibrous capsule is sometimes observed as collagen type III remodels into collagen type I in mature fibrosis [56]. Although collagen type I is the major component of fibrous capsules, collagen type III and type V may also be present. Therefore, future incorporation of multiple siRNAs into nanofibers for controlling these collagens might be an alternative approach to be more effective in preventing fibrous capsule formation. Future experiments to measure the *in vivo* siRNA release profile and to evaluate the *in vivo* efficiency of COL1A1 silencing with respect to endogenous expression would also be conducted to provide informative assessment on the applicability of this gene-silencing platform.

Cell infiltration into the scaffolds is essential for a range of tissue-engineering applications. Contrary to the lack of *in vitro* cell infiltration that is frequently reported in electrospun scaffolds [58], we observed a degree of cell infiltration into PCLEEP nanofiber scaffolds. Such cell infiltration was also observed in our previous study [27]. However, in the latter case, complete cell infiltration was seen as early as 1-week post implantation. It is possible that variations in chemistry and hydrophilicity of the polymers may have contributed to the difference in cell infiltration [59, 60]. However, the exact reasons remain to be elucidated with further detailed studies. In addition, no significant difference in cell infiltration was observed for siCOL1A/CPP, siCOL1A1/TKO and PCLEEP samples. This suggested that siRNA, CPP and TKO molecules did not alter tissue-scaffold integration.

5. Conclusion

This paper demonstrates 'proof of concept' of the reduction in fibrous capsule thickness through the down-regulation of collagen type I and the feasibility of delivering siCOL1A1 and CPP complexes within nanofiber constructs for scaffold-mediated long-term gene silencing applications. By encapsulating siRNA/CPP complexes within PCLEEP fibers, a sustained release of siRNA was obtained for at least 28 days. In contrast to conventional bolus delivery of siRNA, the sustained availability of siRNA from nanofibers prolonged *in vitro* silencing of collagen type I production by 2–3 times. In addition, a significant decrease in *in vivo* fibrous capsule formation was observed around siCOL1A1/CADY and siCOL1A1/TKO samples at weeks 2 and 4. Such combination of gene-silencing approach with biomimicking nanofibers may find useful applications in regenerative medicine for controlling fibrous capsule formation.

Supplementary Material

Refer to Web version on PubMed Central for supplementary material.

Acknowledgments

The partial funding support from AStar BMRC SSCC grant (09/016), MOE AcRF Tier One grant (RG75/10), NIH grant (NIBIB EB006365-07-A2) and the National Basic Research Program of China (973 Program, 2010CB934000) are acknowledged.

References

1. Ratner BD. Reducing capsular thickness and enhancing angiogenesis around implant drug release systems. Journal of Controlled Release. 2002; 78:211–218. [PubMed: 11772462]
2. Anderson JM. Biological responses to materials. Annual Review of Materials Research. 2001; 31:81–110.
3. Hashemi SM, Soudi S, Shabani I, Naderi M, Soleimani M. The promotion of stemness and pluripotency following feeder-free culture of embryonic stem cells on collagen-grafted 3-dimensional nanofibrous scaffold. Biomaterials. 2011; 32:7363–7374. [PubMed: 21762983]
4. Fawcett JW, Asher RA. The glial scar and central nervous system repair. Brain Research Bulletin. 1999; 49:377–391. [PubMed: 10483914]
5. Destouet JM, Monsees BS, Oser RF, Nemecek JR, Young VL, Pilgram TK. Screening mammography in 350 women with breast implants: prevalence and findings of implant complications. American Journal of Roentgenology. 1992; 159:973. [PubMed: 1414810]
6. Joseph J, Mohanty M, Mohanan PV. Role of immune cells and inflammatory cytokines in regulation of fibrosis around silicone expander implants. Journal of Materials Science-Materials in Medicine. 2010; 21:1665–1676. [PubMed: 20162333]
7. Wisniewski N, Moussy F, Reichert WM. Characterization of implantable biosensor membrane biofouling. Fresenius' Journal of Analytical Chemistry. 2000; 366:611–621. [PubMed: 11225773]

8. Zhao Q, Topham N, Anderson JM, Hiltner A, Lodoen G, Payet CR. Foreign-body giant cells and polyurethane biostability: In vivo correlation of cell adhesion and surface cracking. Journal of Biomedical Materials Research. 1991; 25:177–183. [PubMed: 2055915]
9. Shen MC, Horbett TA. The effects of surface chemistry and adsorbed proteins on monocyte/macrophage adhesion to chemically modified polystyrene surfaces. J Biomed Mater Res. 2001; 57:336–345. [PubMed: 11523028]
10. Ward WK, Slobodzian EP, Tiekotter KL, Wood MD. The effect of microgeometry, implant thickness and polyurethane chemistry on the foreign body response to subcutaneous implants. Biomaterials. 2002; 23:4185–4192. [PubMed: 12194521]
11. Sanders JE, Lamont SE, Karchin A, Golledge SL, Ratner BD. Fibro-porous meshes made from polyurethane microfibers: effects of surface charge on tissue response. Biomaterials. 2005; 26:813–818. [PubMed: 15350787]
12. Klosterhalfen B, Junge K, Klinge U. The lightweight and large porous mesh concept for hernia repair. Expert Review of Medical Devices. 2005; 2:103–117. [PubMed: 16293033]
13. Zuniga J, Fuenzalida M, Guerrero A, Illanes J, Dabancens A, Diaz E, et al. Effects of steroidal and non steroidal drugs on the neovascularization response induced by tumoral TA3 supernatant on CAM from chick embryo. Biological Research. 2003; 36:233–240. [PubMed: 14513718]
14. Norton LW, Tegnell E, Toporek SS, Reichert WM. In vitro characterization of vascular endothelial growth factor and dexamethasone releasing hydrogels for implantable probe coatings. Biomaterials. 2005; 26:3285–3297. [PubMed: 15603824]
15. Patil SD, Papadmitrakopoulos F, Burgess DJ. Concurrent delivery of dexamethasone and VEGF for localized inflammation control and angiogenesis. Journal of Controlled Release. 2007; 117:68–79. [PubMed: 17169457]
16. Ravin AG, Olbrich KC, Levin LS, Usala AL, Klitzman B. Long- and short-term effects of biological hydrogels on capsule microvascular density around implants in rats. J Biomed Mater Res. 2001; 58:313–318. [PubMed: 11319747]
17. Luo JC, Shin VY, Liu ESL, Ye YN, Wu WKK, So WHL, et al. Dexamethasone delays ulcer healing by inhibition of angiogenesis in rat stomachs. European Journal of Pharmacology. 2004; 485:275–281. [PubMed: 14757151]
18. Chigurupati S, Kulkarni T, Thomas S, Shah G. Calcitonin stimulates multiple stages of angiogenesis by directly acting on endothelial cells. Cancer Research. 2005; 65:8519–8529. [PubMed: 16166333]
19. Hu W, Lu CH, Han HD, Huang J, Shen DY, Stone RL, et al. Biological roles of the delta family notch ligand Dll4 in tumor and endothelial cells in ovarian cancer. Cancer Research. 2011; 71:6030–6039. [PubMed: 21795478]
20. Stany MP, Vathipadiekal V, Ozbun L, Stone RL, Mok SC, Xue H, et al. Identification of novel therapeutic targets in microdissected clear cell ovarian cancers. PLoS ONE. 2011; 6
21. Samakoglu S, Lisowski L, Budak-Alpdogan T, Usachenko Y, Acuto S, Di Marzo R, et al. A genetic strategy to treat sickle cell anemia by coregulating globin transgene expression and RNA interference. Nat Biotechnol. 2006; 24:89–94. [PubMed: 16378095]
22. Leachman SA, Hickerson RP, Schwartz ME, Bullough EE, Hutcherson SL, Boucher KM, et al. First-in-human mutationtargeted siRNA phase Ib trial of an inherited skin disorder. Molecular Therapy. 2010; 18:442–446. [PubMed: 19935778]
23. Cao HQ, Jiang X, Chai C, Chew SY. RNA interference by nanofiber-based siRNA delivery system. Journal of Controlled Release. 2010; 144:203–212. [PubMed: 20138939]
24. Rujitanaroj PO, Wang YC, Wang J, Chew SY. Nanofiber-mediated controlled release of siRNA complexes for long term gene-silencing applications. Biomaterials. 2011; 32:5915–5923. [PubMed: 21596430]
25. Bashur CA, Shaffer RD, Dahlgren LA, Guelcher SA, Goldstein AS. Effect of fiber diameter and alignment of electrospun polyurethane meshes on mesenchymal progenitor cells. Tissue Engineering Part A. 2009; 15:2435–2445. [PubMed: 19292650]
26. Chew SY, Mi R, Hoke A, Leong KW. The effect of the alignment of electrospun fibrous scaffolds on Schwann cell maturation. Biomaterials. 2008; 29:653–661. [PubMed: 17983651]

27. Cao HQ, McHugh K, Chew SY, Anderson JM. The topographical effect of electrospun nanofibrous scaffolds on the in vivo and in vitro foreign body reaction. Journal of Biomedical Materials Research Part A. 2010; 93A:1151–1159. [PubMed: 19768795]

28. Takahashi H, Wang YW, Grainger DW. Device-based local delivery of siRNA against mammalian target of rapamycin (mTOR) in a murine subcutaneous implant model to inhibit fibrous encapsulation. Journal of Controlled Release. 2010; 147:400–407. [PubMed: 20727922]

29. Moschos SA, Jones SW, Perry MM, Williams AE, Erjefalt JS, Turner JJ, et al. Lung delivery studies using siRNA conjugated to TAT (48- 60) and penetratin reveal peptide induced reduction in gene expression and induction of innate immunity. Bioconjugate Chem. 2007; 18:1450–1459.

30. Simeoni F, Morris MC, Heitz F, Divita G. Insight into the mechanism of the peptide-based gene delivery system MPG: implications for delivery of siRNA into mammalian cells. Nucl Acids Res. 2003; 31:2717–2724. [PubMed: 12771197]

31. Crombez L, Aldrian-Herrada G, Konate K, Nguyen QN, McMaster GK, Brasseur R, et al. A new potent secondary amphipathic cell-penetrating peptide for siRNA delivery into mammalian cells. Molecular Therapy. 2009; 17:95–103. [PubMed: 18957965]

32. Davidson TJ, Harel S, Arboleda VA, Prunell GF, Shelanski ML, Greene LA, et al. Highly efficient small interfering RNA delivery to primary mammalian neurons induces microRNA-like effects before mRNA degradation. J Neurosci. 2004; 24:10040–10046. [PubMed: 15537872]

33. Lundberg P, El-Andaloussi S, Sutlu T, Johansson H, Langel U. Delivery of short interfering RNA using endosomolytic cell-penetrating peptides. FASEB J. 2007; 21:2664–2671. [PubMed: 17463227]

34. Crombez L, Morris MC, Dufort S, Aldrian-Herrada G, Nguyen Q, Mc Master G, et al. Targeting cyclin B1 through peptide-based delivery of siRNA prevents tumour growth. Nucleic Acids Research. 2009; 37:4559. [PubMed: 19483097]

35. Moschos S, Williams A, Lindsay M. Cell-penetrating-peptide-mediated siRNA lung delivery. Biochemical Society Transactions. 2007; 35:807–810. [PubMed: 17635153]

36. Lehto T, Simonson OE, Mager I, Ezzat K, Sork H, Copolovici DM, et al. A peptide-based vector for efficient gene transfer in vitro and in vivo. Molecular Therapy. 2011; 19:1457–1467. [PubMed: 21343913]

37. Bell H, Kimber WL, Li MW, Whittle IR. Liposomal transfection efficiency and toxicity on glioma cell lines: in vitro and in vivo studies. Neuroreport. 1998; 9:793–798. [PubMed: 9579667]

38. Andersen MO, Howard KA, Paludan SR, Besenbacher F, Kjems J. Delivery of siRNA from lyophilized polymeric surfaces. Biomaterials. 2008; 29:506–512. [PubMed: 17950838]

39. Beyerle A, Irmler M, Beckers J, Kissel T, Stoeger T. Toxicity pathway focused gene expression profiling of PEI-based polymers for pulmonary applications. Mol Pharm. 2010; 7:727–737. [PubMed: 20429563]

40. Moghimi SM, Symonds P, Murray JC, Hunter AC, Debska G, Szewczyk A. A two-stage poly(ethylenimine)-mediated cytotoxicity: Implications for gene transfer/therapy. Molecular Therapy. 2005; 11:990–995. [PubMed: 15922971]

41. Xiao CS, Wang YC, Du JZ, Chen XS, Wang J. Kinetics and mechanism of 2-ethoxy-2-oxo-1,3,2-dioxaphospholane polymerization initiated by stannous octoate. Macromolecules. 2006; 39:6825–6831.

42. Wang YC, Li Y, Yang XZ, Yuan YY, Yan LF, Wang J. Tunable thermosensitivity of biodegradable polymer micelles of poly (epsilon-caprolactone) and polyphosphoester block copolymers. Macromolecules. 2009; 42:3026–3032.

43. Simeoni F, Morris MC, Heitz F, Divita G. Peptide-based strategy for siRNA delivery into mammalian cells. Methods Mol Biol. 2005; 309:251–260. [PubMed: 15990405]

44. Voskerician G, Shive MS, Shawgo RS, von Recum H, Anderson JM, Cima MJ, et al. Biocompatibility and biofouling of MEMS drug delivery devices. Biomaterials. 2003; 24:1959–1967. [PubMed: 12615486]

45. Voskerician G, Gingras PH, Anderson JM. Macroporous condensed poly(tetrafluoroethylene). I. in vivo inflammatory response and healing characteristics. Journal of Biomedical Materials Research Part A. 2006; 76A:234–242. [PubMed: 16116600]

46. Chew SY, Mi RF, Hoke A, Leong KW. Aligned protein-polymer composite fibers enhance nerve regeneration: a potential tissue-engineering platform. Advanced Functional Materials. 2007; 17:1288–1296. [PubMed: 18618021]
47. Choi JS, Lee SJ, Christ GJ, Atala A, Yoo JJ. The influence of electrospun aligned poly(epsilon-caprolactone)/collagen nanofiber meshes on the formation of self-aligned skeletal muscle myotubes. Biomaterials. 2008; 29:2899–2906. [PubMed: 18400295]
48. Yu WW, Zhao W, Zhu C, Zhang XL, Ye DX, Zhang WJ, et al. Sciatic nerve regeneration in rats by a promising electrospun collagen/poly(epsilon-caprolactone) nerve conduit with tailored degradation rate. BMC Neurosci. 2011; 12
49. Zhu YQ, Wang AJ, Patel S, Kurpinski K, Diao E, Bao X, et al. Engineering bi-layer nanofibrous conduits for peripheral nerve regeneration. Tissue Engineering Part C-Methods. 2011; 17:705–715. [PubMed: 21501089]
50. Ravichandran R, Ng CCH, Liao S, Pliszka D, Raghunath M, Ramakrishna S, et al. Biomimetic surface modification of titanium surfaces for early cell capture by advanced electrospinning. Biomedical Materials. 2012; 7
51. Yang J, Kim DH, Hendricks JL, Leach M, Northey R, Martin DC. Ordered surfactant-templated poly(3,4- ethylenedioxythiophene) (PEDOT) conducting polymer on microfabricated neural probes. Acta Biomaterialia. 2005; 1:125–136. [PubMed: 16701786]
52. Morris MC, Chaloin L, Mery J, Heitz F, Divita G. A novel potent strategy for gene delivery using a single peptide vector as a carrier. Nucleic Acids Res. 1999; 27:3510–3517. [PubMed: 10446241]
53. Jang JH, Bengali Z, Houchin TL, Shea LD. Surface adsorption of DNA to tissue engineering scaffolds for efficient gene delivery. Journal of Biomedical Materials Research Part A. 2006; 77A: 50–58. [PubMed: 16353173]
54. Holladay C, Keeney M, Greiser U, Murphy M, O'Brien T, Pandit A. A matrix reservoir for improved control of nonviral gene delivery. Journal of Controlled Release. 2009; 136:220–225. [PubMed: 19233237]
55. Xie JW, Wang CH. Electrospun micro- and nanofibers for sustained delivery of paclitaxel to treat C6 glioma in vitro. Pharm Res. 2006; 23:1817–1826. [PubMed: 16841195]
56. Darby, IA.; Hewitson, TD. Fibroblast differentiation in wound healing and fibrosis. In: Jeon, KW., editor. International Review of Cytology - a Survey of Cell Biology. 2007. p. 143
57. Shegogue D, Trojanowska M. Mammalian target of rapamycin positively regulates collagen type I production via a phosphatidylinositol 3-kinase-independent pathway. Journal of Biological Chemistry. 2004; 279:23166–23175. [PubMed: 15047702]
58. Dahlin RL, Kasper FK, Mikos AG. Polymeric nanofibers in tissue engineering. Tissue Engineering Part B-Reviews. 2011; 17:349–364. [PubMed: 21699434]
59. Rnjak-Kovacina J, Weiss AS. Increasing the pore size of electrospun scaffolds. Tissue Engineering Part B-Reviews. 2011; 17:365–372. [PubMed: 21815802]
60. Vaquette C, Cooper-White JJ. Increasing electrospun scaffold pore size with tailored collectors for improved cell penetration. Acta Biomaterialia. 2011; 7:2544–2557. [PubMed: 21371575]

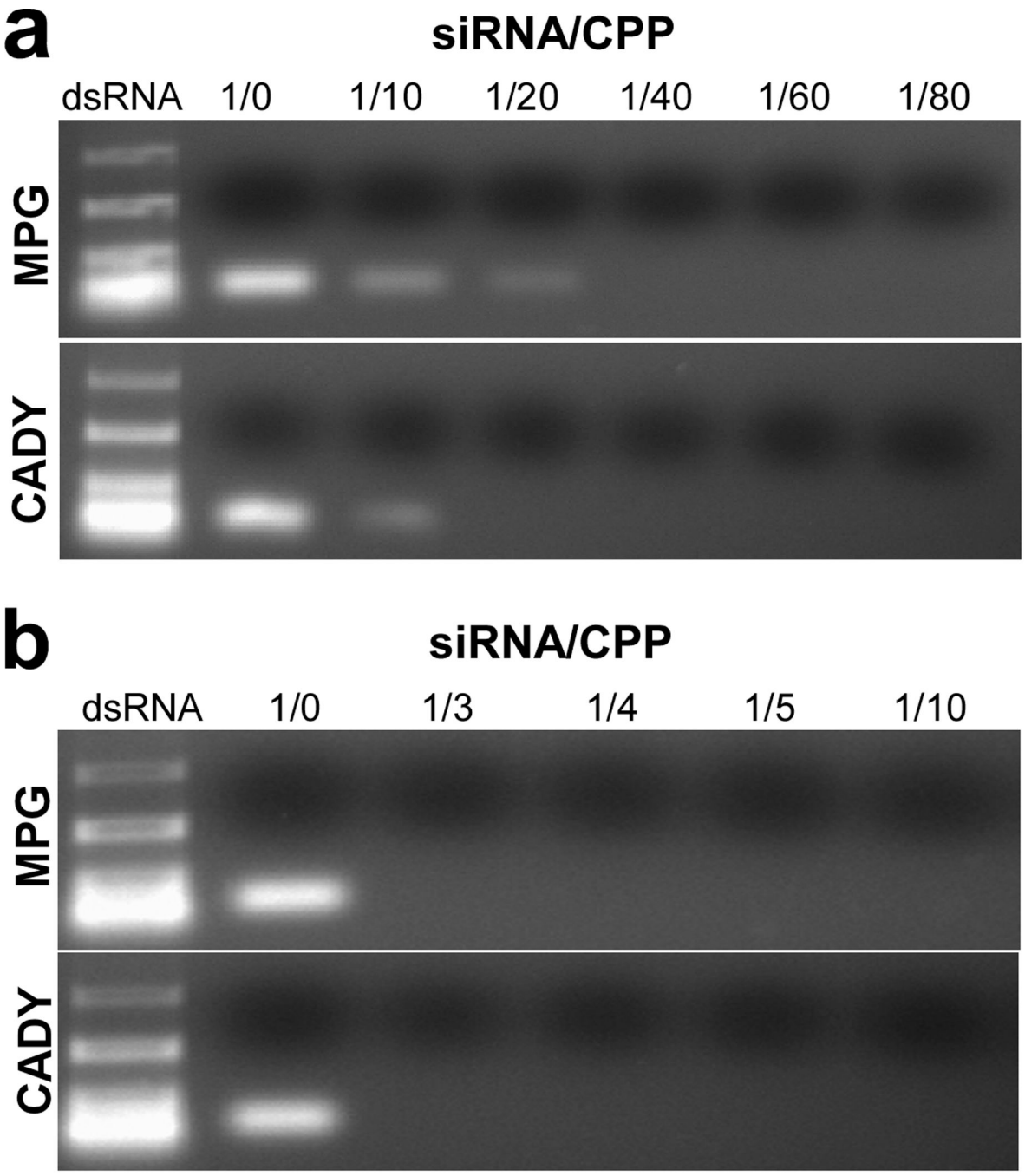

Fig. 1.
Agarose gel shift assay for siRNA/CPP complexes with varying (a) molar ratios between 1/0 and 1/80 and (b) volume ratios between 1/0 and 1/10. White bands show the migration of siRNA.

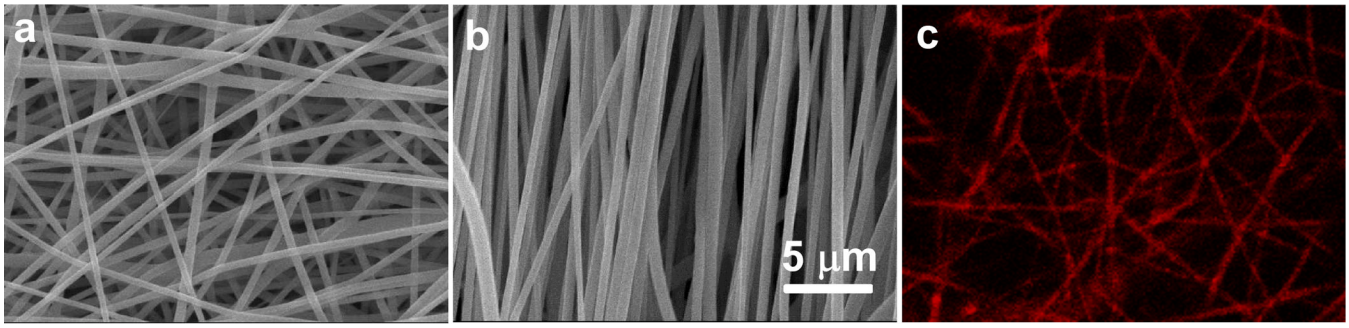

Fig. 2.
SEM images of siCOL1A1/CADY-encapsulated PCLEEP nanofibers with (a) random, (b) aligned orientations and (c) distribution of Cy5-ODN (red color) from Cy5-ODN/CADY complexes within nanofibers, depicting uniform and bead-free fibers.

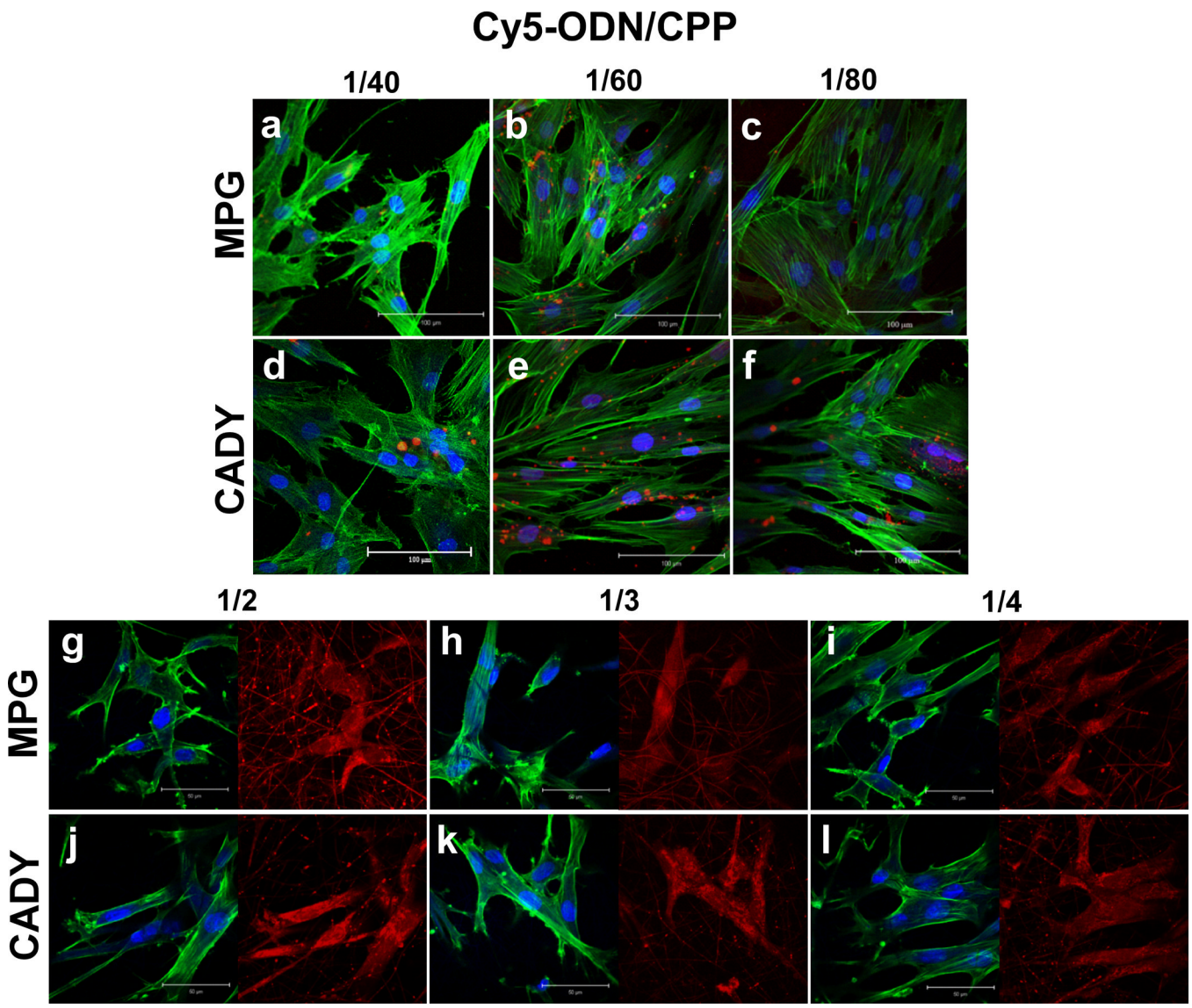

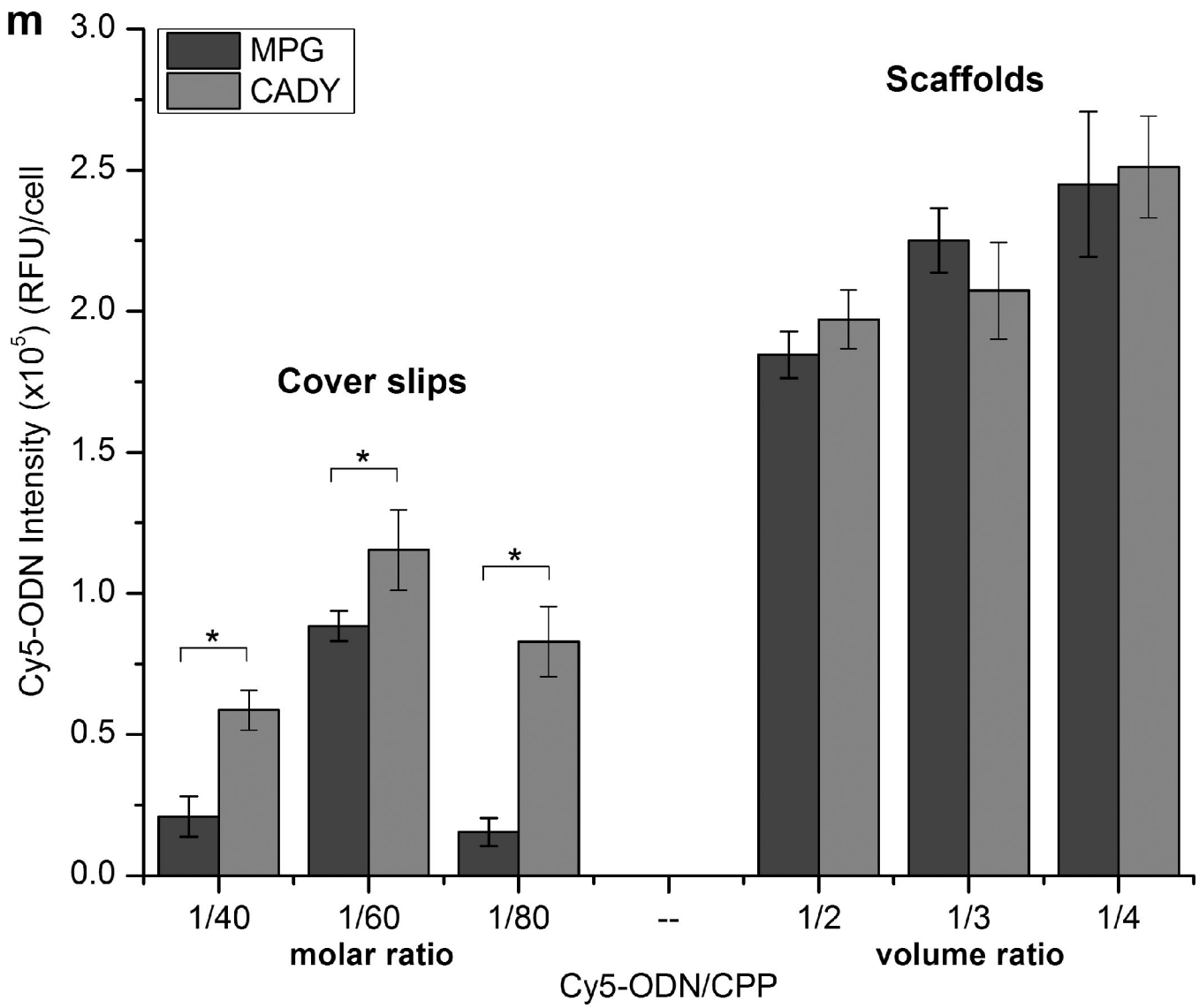

Fig. 3.

Cy5-ODN uptake by HDFs. (a-f) Cells were seeded on glass cover slips (control) with the Cy5-ODN/CPP complexation at molar ratios between 1/40 and 1/80. Scale bar = 100 μm. (g–l) Cells were seeded on Cy5-ODN/CPP scaffolds at volume ratios between 1/2 and 1/4. Scale bar = 50 μm. Pseudo color red indicates the distribution of Cy5-ODN, blue signals present cell nuclei by DAPI staining and green signals show cytoskeleton by Phalloidin staining. (m) Quantitative analysis of Cy5 signal intensity revealed significantly higher Cy5-ODN uptake on scaffolds than on cover slips. * indicates $p < 0.05$.

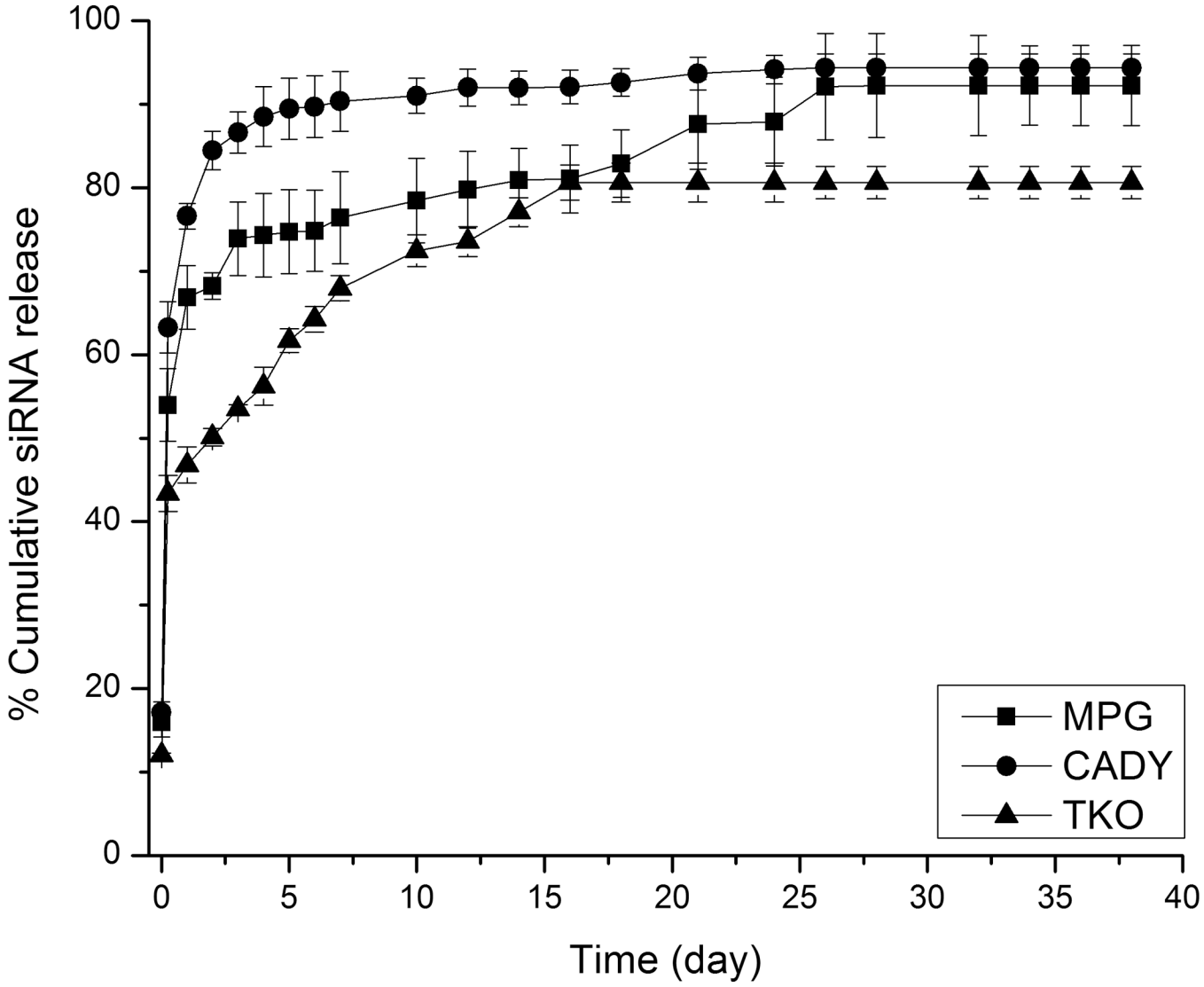

Fig. 4.

In vitro release kinetics of siRNA/MPG, siRNA/CADY, and siRNA/TKO complexes from PCLEEP nanofibers as observed in PBS at 37 °C.

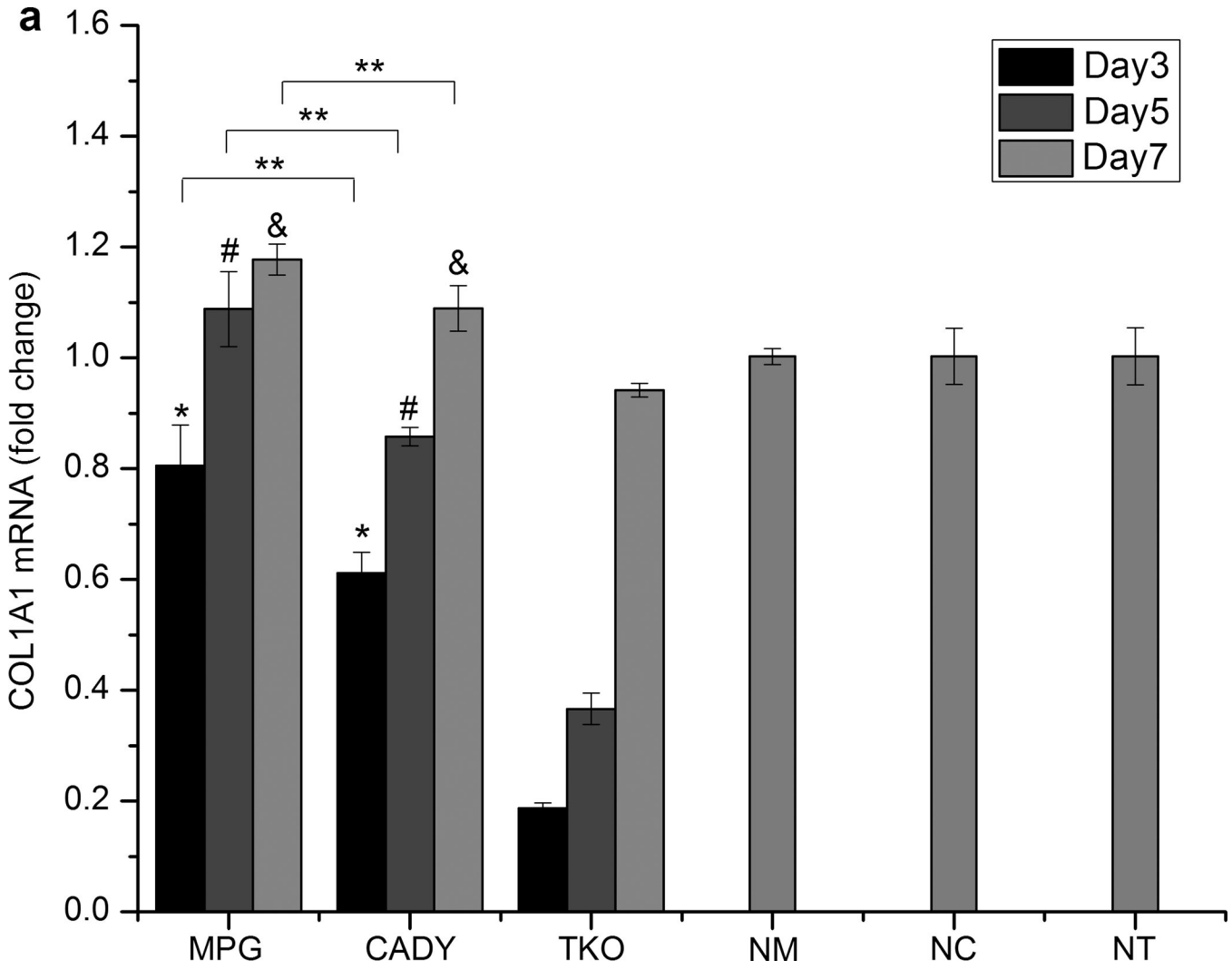

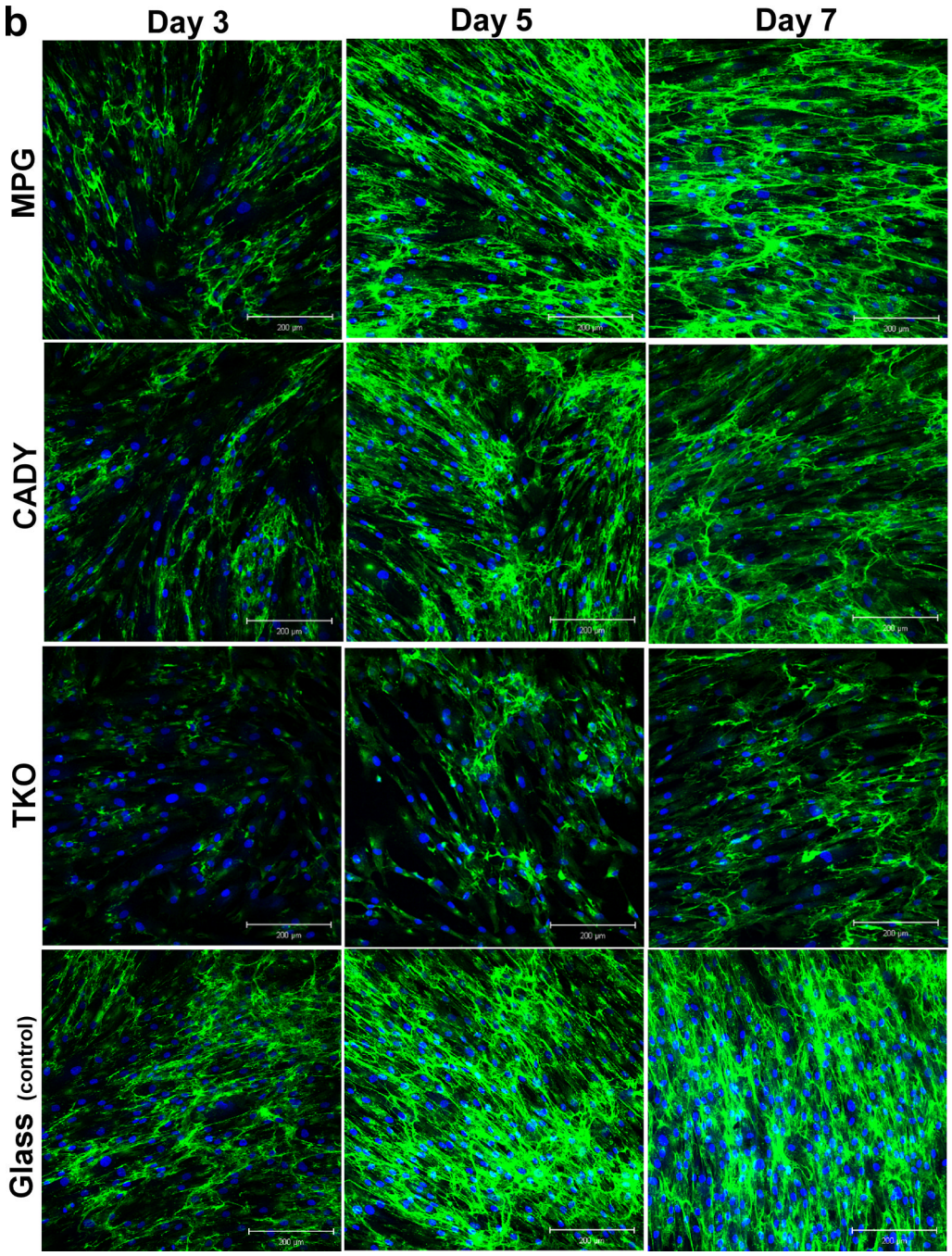

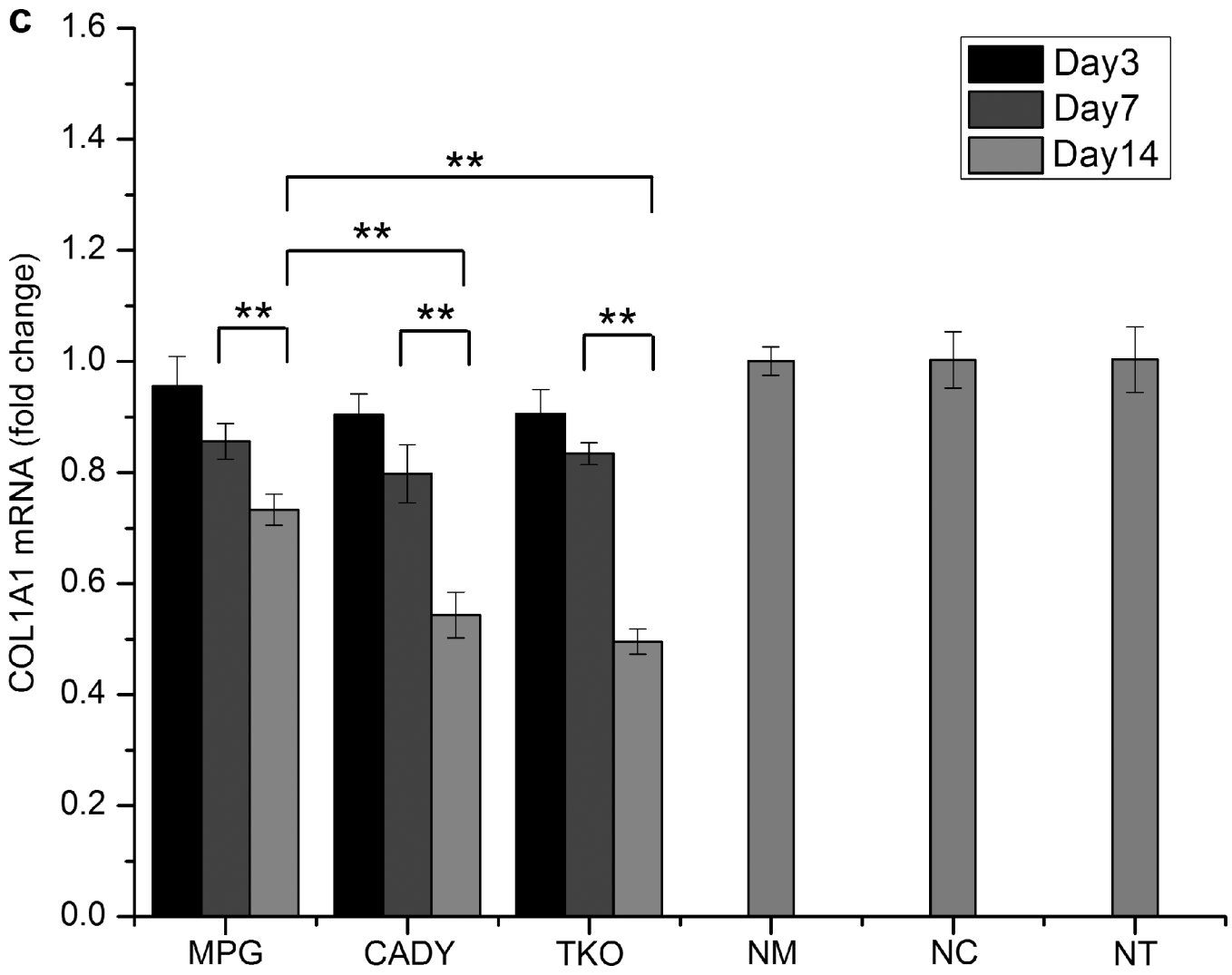

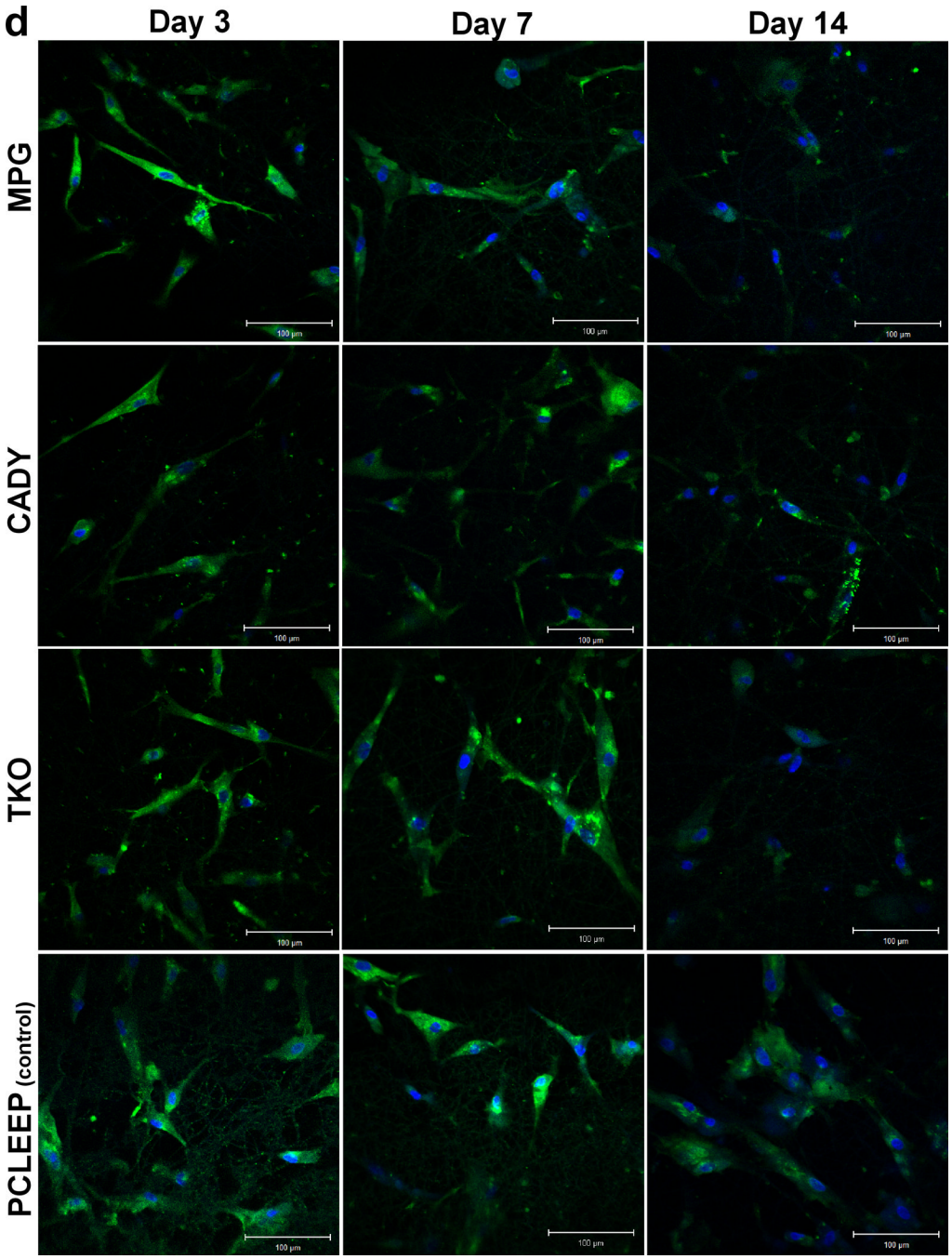

Fig. 5.

Long-term COL1A1 knockdown efficiency and immunofluorescence analysis by (a,b) bolus delivery and (c,d) scaffold-mediated delivery. (a,c) COL1A1 mRNA expression levels in transfected HDF cells and (b,d) collagen immunofluorescense of transfected HDF cells. *, #, and & indicate $p < 0.05$ as compared to TKO samples at each time point. ** indicates $p < 0.05$. n = 3, mean ± *SE*. NM, NC and NT denote the negative controls for MPG, CADY and TKO which comprised of cells treated with siNEG/MPG, siNEG/CADY and siNEG/TKO respectively.

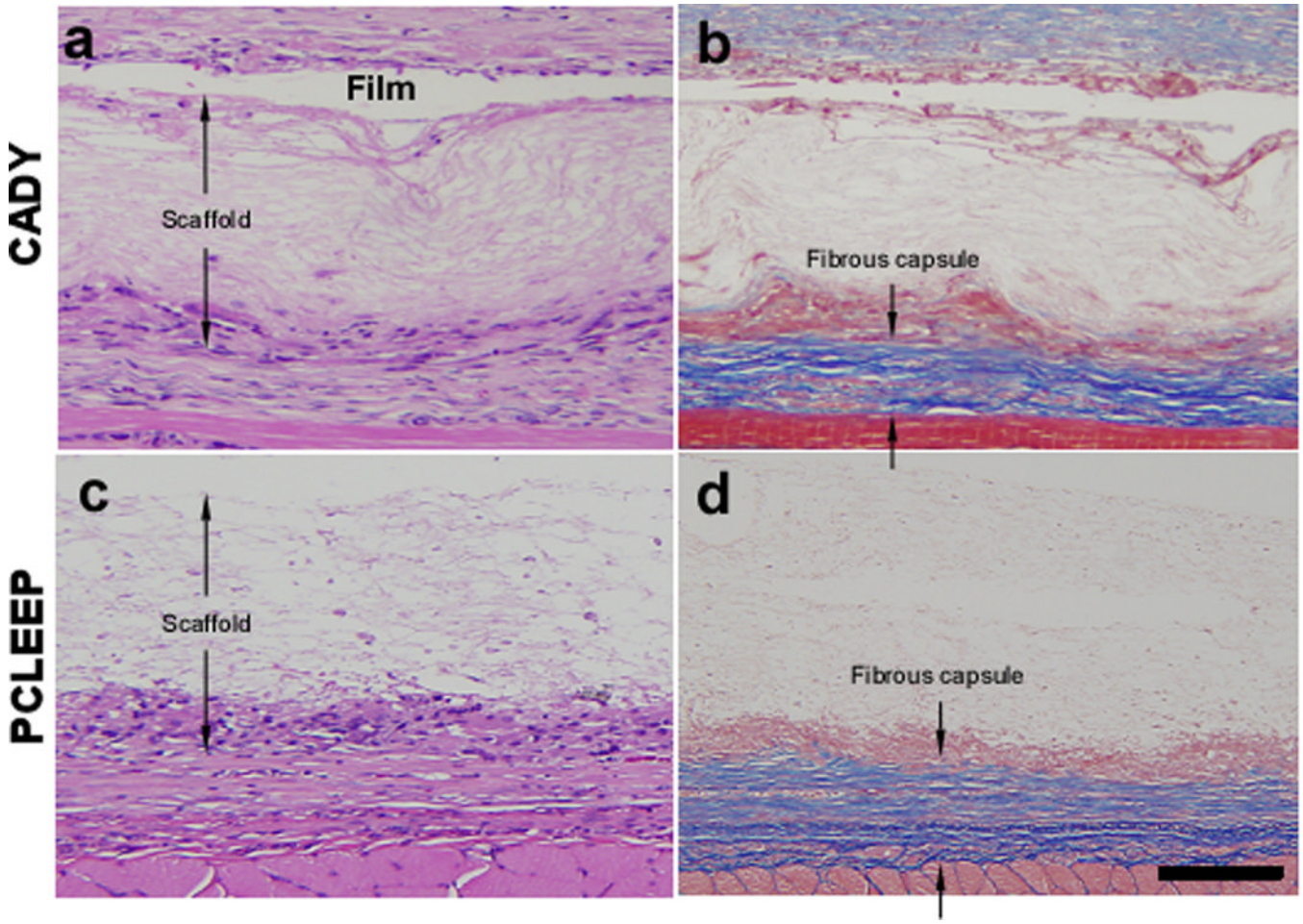

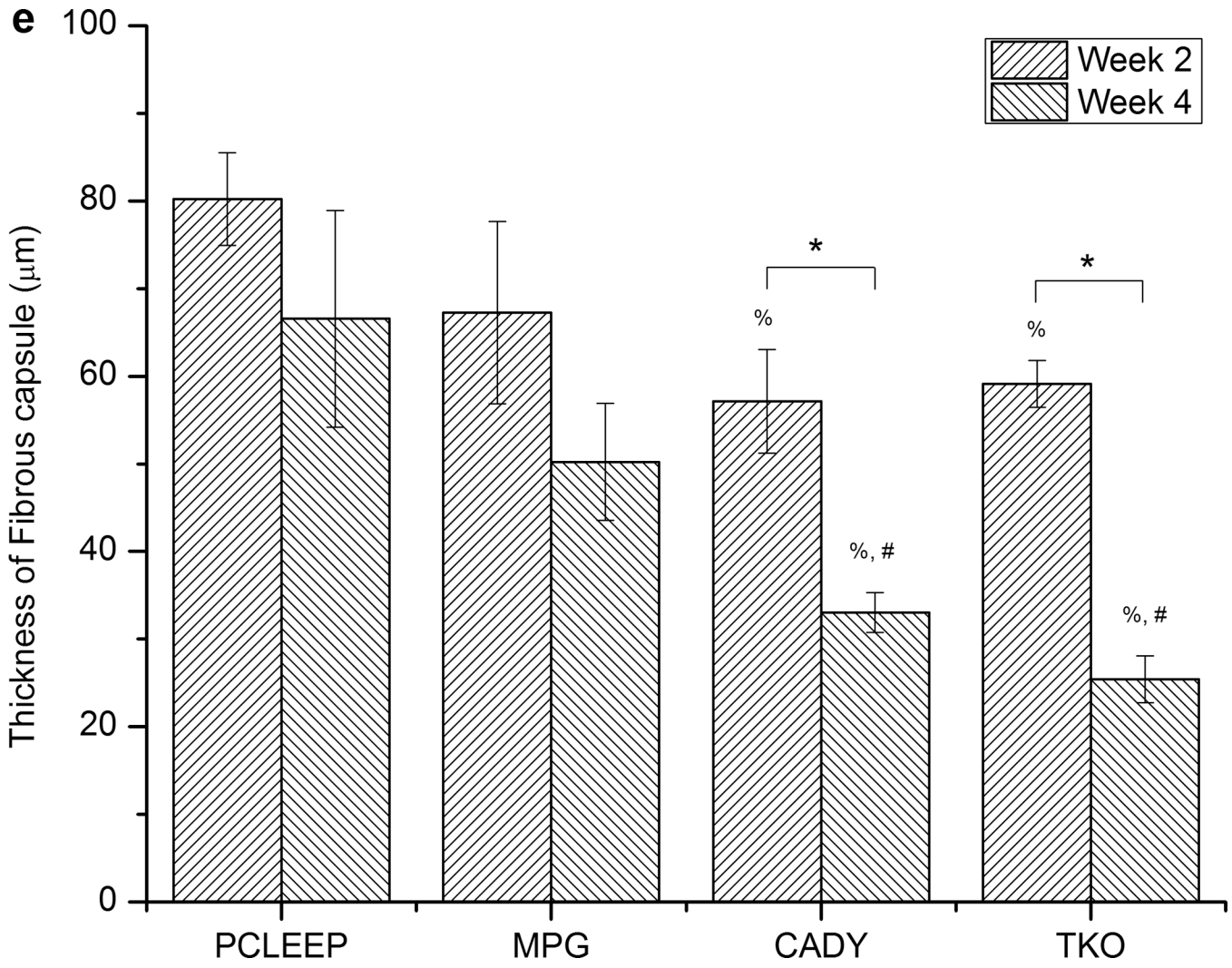

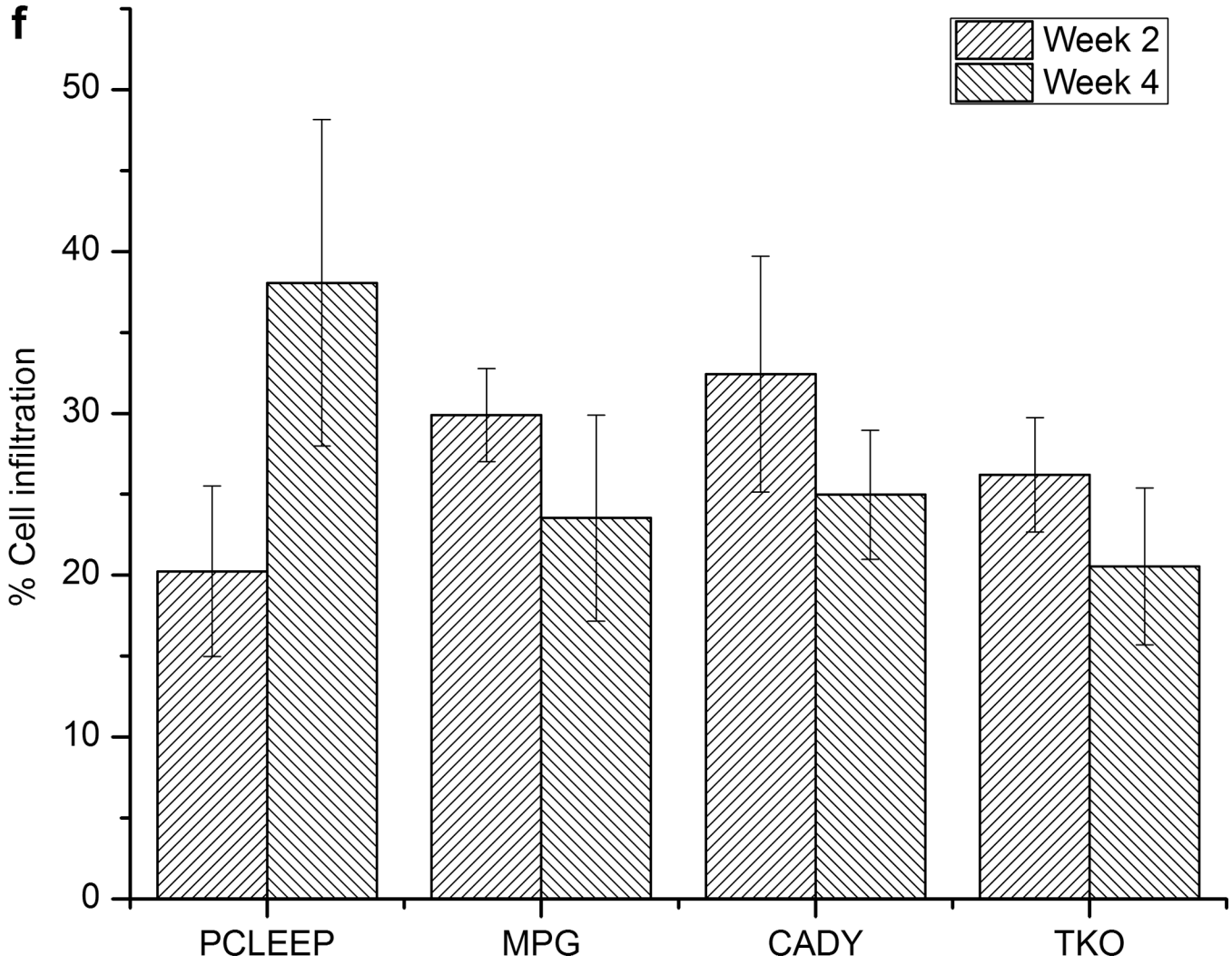

Fig. 6.

Histological images showing the fibrous capsule formation and cell infiltration on aligned nanofibers scaffolds that were supported on films at week 4 with H and E staining (left) and Masson's Trichrome staining (right). (a,b) siCOL1A1/CADY and (c,d) PCLEEP samples. Distance between the arrowheads indicates the thickness of the aligned scaffold (without film) with cell infiltration and the thickness of fibrous capsule. Quantitative analysis of (e) fibrous capsule thickness and (f) cell infiltration. * indicates $p < 0.05$, unpaired T-test. % indicates $p < 0.05$, Mann-Whitney Test as compared to PCLEEP. # indicates $p < 0.05$, Mann-Whitney Test as compared to siCOL1A1/MPG. n = 90, mean ± *SE*. The scale bar is 100 μm.

Table 1

Processing parameters for siRNA-nanofiber scaffolds

Samples	Volume ratio[a]	Equivalent molar ratio[b]	Electrospinning parameters	
			Random fibers	Aligned fibers[d]
siCOL1A1/MPG, siNEG/MPG	1/2	1/15	+12/-4 kV 1.5 mL/h 12 cm[c] 5 × 5 cm^2	-
	1/3	1/20		-
	1/4	1/30		2500 rpm[e]
siCOL1A1/CADY, siNEG/CADY	1/2	1/15		-
	1/3	1/20		-
	1/4	1/30		2500 rpm[e]
siCOL1A1/TKO, siNEG/TKO	1/2	1/15		2500 rpm[e]
PCLEEP (plain fibers)	-	-		

[a] Volume ratios of 1/2 (15μL/30μL), 1/3 (15μL/45μL) and 1/4 (15μL/60μL)

[b] Conversion of volume ratios to molar ratios

[c] Distance from needle tip to collector surface

[d] All parameters were the same as random fibers except for the inclusion of a grounded rotating target

[e] A grounded rotating target